Generalized hydrodynamics and dispersion relations in lattice gases

S. P. Das
Theoretical Physics Division, Bhabha Atomic Research Centre, Trombay, Bombay 400 085, India

H. J. Bussemaker and M. H. Ernst
Institute for Theoretical Physics, Princetonplein 5, P.O. Box 80006, 3508 TA Utrecht, The Netherlands
(15 December 1992; revised manuscript received 1 March 1993)

Spectra or decay rates of spatial fluctuations are calculated from mean-field theory or Boltzmann's equation for thermal and athermal lattice-gas automata, with the emphasis on long-lived hydrodynamic modes. The spectra provide information on isotropy, existence of spurious conservation laws, and time and length scales of hydrodynamic behavior. Particularly important is the range of validity of generalized hydrodynamics with wave-number-dependent sound speed and transport coefficients. These properties give a quantitative explanation of several existing, but unexplained simulation results on the so-called negative bulk viscosities, and on the strong dispersion in the simulation results on sound damping.

PACS number(s): 05.20.Dd, 05.50.+q, 05.60.+w

I. INTRODUCTION

Spontaneous spatial fluctuations around equilibrium in real fluids and lattice gases decay on the average as $\exp[z_\lambda(\mathbf{k})t]$, and so do small macroscopic deviations from equilibrium. The different decay modes λ at wave number $\mathbf{k}$ are the shear, heat, and sound modes, as well as kinetic modes. In this paper we study the spectra or hydrodynamic dispersion relations $z_\lambda(\mathbf{k})$ of spatial fluctuations in the occupations of single-particle states, which provide basic information about the collective excitations and their relevant time and length scales. The spectra show how the speed of sound, damping constants, and transport coefficients depend on the wavelength of the excitations, on the thermodynamic variables, and on the microscopic details of the models. In this manner we are able to develop important and practical criteria to judge the applicability of lattice-gas models for the study of flow properties and thermal effects in nonequilibrium fluids.

The set of (real parts of) eigenvalues determines the basic set of relaxation constants or time scales in the problem. Given the frequency or wavelength of interest one can judge from the spectrum which eigenmodes of the kinetic equation are relevant. In the *hydrodynamic regime* of fluids the wavelengths and time scales of interest are large compared to all correlation lengths (range of interaction, lattice distance, mean free path ℓ_0), and microscopic times (collision time, mean free time $t_0 = 1/\omega_0$). This case is mostly relevant for scattering experiments on fluids, where the Landau-Placzek theory fully explains the dynamic scattering function $S(\mathbf{k},\omega)$ on the basis of the slow hydrodynamic modes [1]. As the density decreases one enters into the *kinetic regime*, where the typical wavelengths and time scales are on the order of the mean free path $\ell_0 \sim 1/\rho$ and the mean free time $t_0 = 1/\omega_0$, respectively. Here one needs to include kinetic modes with eigenvalues on the order of ω_0. This case is typical for gases under normal pressure and temperatures [1]. Upon further reduction of the density the wavelengths become small compared to ℓ_0, and one enters in the *free-particle regime*, relevant for Knudsen gases. We will also consider crossover between these three regimes.

In the literature so far only the spectrum of one particular lattice gas has been discussed [2], but no systematic analysis has been presented of the implications of these spectra for the fluid properties of lattice gases. In the present paper the main emphasis is on the hydrodynamic part of the spectrum. On large space and time scales one expects that the hydrodynamic eigenvalues $z_\lambda(\mathbf{k})$ are independent of the details of the rather primitive microscopic dynamics of lattice gases.

A spatial fluctuation has the general form $\delta f(\mathbf{r},\mathbf{c},t) = \psi_\lambda(\mathbf{k},\mathbf{c})\exp[i\mathbf{k}\cdot\mathbf{r} + z_\lambda(\mathbf{k})t]$. The requirement that δf satisfies the linearized kinetic equation in mean-field approximation leads to an eigenvalue equation, the solution of which yields the eigenvalues $z_\lambda(\mathbf{k})$. If the imaginary part, $\mathrm{Im}\, z_\lambda(\mathbf{k}) = c_s(\mathbf{k})k$ is nonvanishing, the excitation propagates with a speed $c_s(\mathbf{k})$. The real part $\mathrm{Re}\, z_\lambda(\mathbf{k}) < 0$ represents damping. Unstable modes correspond to $\mathrm{Re}\, z_\lambda(\mathbf{k}) > 0$. The long-wavelength excitations ($k \to 0$) are either *soft* hydrodynamic modes, related to conservation laws, with $\mathrm{Re}\, z_\lambda(\mathbf{k}) \sim O(k^2)$ or *hard* (rapidly decaying) kinetic modes with $\mathrm{Re}\, z_\lambda(0) < 0$. Apart from the detailed description of standard hydrodynamics the spectra of slow excitations in lattice gases provide the following type of information about the lattice-gas fluids.

(a) Conservation laws. The standard conservation laws of number, momentum, energy, and possibly of other

quantities are reflected in the spectrum as soft eigenvalues with Re $z_\lambda(0) = 0$. In addition the spectrum may show soft modes at a finite wave number k_0, with Re $z_\lambda(\mathbf{k}_0) = 0$. The occurrence of such soft modes reveals the existence of the spurious conservation laws. The best-known examples are the staggered momentum densities [3] and the staggered number densities [4,5]. These modes are soft near a wave number $\mathbf{k}_0$ equal to half a reciprocal lattice vector.

(b) Isotropy. The symmetries of the lattice gas's dynamic equations are discrete, not continuous. In order to model the nonlinear Navier-Stokes equations of isotropic fluids by lattice gases one has to require that the fourth-rank viscosity tensor be isotropic, at least to $O(u^2)$ in the fluid flow velocity $\mathbf{u}$ as $u \to 0$. This condition is very restrictive as to the type of regular space lattices allowed in the construction of lattice gases. In fact, in two (four) dimensions only the triangular lattice [face-centered hypercubic (FCHC) lattice] has the required symmetry. In three dimensions there does not exist any lattice with isotropic fourth-rank tensors [6]. Any fourth-rank tensor (such as viscosity) on a lattice with inversion and reflection symmetries contains in general *three* independent scalars (bulk, shear, and cubic viscosity). On triangular and FCHC lattices and in isotropic systems the shear and cubic viscosity coincide. This manifests itself in a twofold degeneracy of a kinetic eigenvalue $z_\lambda(0) \neq 0$, whereas for finite $\mathbf{k}$ values this degeneracy is lifted, as we shall see. Another aspect of isotropy of the hydrodynamic equations in real fluids is that the spectra are independent of the direction of $\mathbf{k}$, i.e., $z_\lambda(\mathbf{k}) = z_\lambda(k)$. Of course, isotropy in lattice gases is an idealization, a limiting property, that can only be valid approximately at long wavelengths. Furthermore, isotropy in lattice gases is only defined in the restricted sense of applying to tensors of second and fourth rank, but not to any higher-order tensors. At finite $\mathbf{k}$ lattice gases are no longer isotropic and the speed and damping of sound depend on the direction of $\mathbf{k}$ as is the case in crystals, and so do the kinematic viscosity and heat diffusivity.

In the preceding paragraphs we have been emphasizing the parallels with the spectra of isotropic fluids. It is worthwhile to also stress the differences. At finite wave numbers the spectra $z_\lambda(\mathbf{k})$ of lattice gases still exhibit the discrete lattice symmetries, which become more pronounced with increasing k. The eigenvalues are in fact periodic functions in reciprocal $\mathbf{k}$ space, with d independent periods in a d-dimensional lattice. The effects of lattice symmetries are clearly shown in the graphs of the present paper.

(c) Generalized hydrodynamics. There are crossovers between the different regimes described above. The most interesting one for fluids is the regime of generalized hydrodynamics, where there is still a clear separation between the slow hydrodynamic modes and the fast kinetic modes, but *constant* transport coefficients in the linearized hydrodynamic equations are no longer adequate. They should be replaced by transport coefficients that are slowly varying functions of the wave number $\mathbf{k}$. This implies that the relations between irreversible fluxes (heat current, stress tensor) and thermodynamic driving forces (temperature and velocity gradients) are strictly *nonlocal.* The $\mathbf{k}$-dependent transport coefficients can be calculated explicitly from the Boltzmann equation. By investigating the excitation spectrum $z_\lambda(\mathbf{k})$ for different wave numbers one can judge the size of the long-wavelength region where the eigenmodes are hydrodynamic in character with constant transport coefficients. The crossover regime is particularly important in analyzing the transport coefficients measured in computer simulations in lattice gases. Certain unexplained simulation results in the literature [7,8], misleadingly described as a "negative bulk viscosity," are in fact pure effects of generalized hydrodynamics. They can be explained *quantitatively* on the basis of the lattice Boltzmann equation, as will also be shown in this paper. Transport coefficients and damping constants are non-negative.

(d) Spatial instability. A recent and very interesting application of the spectra deals with the dynamics of phase separation in lattice-gas models for thermodynamically unstable systems (spinodal decomposition), as occurring in the long-range Van der Waals–type model of Appert and Zaleski [9,10] or in the biased lattice gas of Refs. [11,12]. Calculations of spectra show that the real part of one or more eigenvalues $z_\lambda(\mathbf{k})$ becomes positive for $|\mathbf{k}| < k_0$, implying that the corresponding modes with a wavelength larger than $2\pi/k_0$ are unstable. The onset of coarsening in spinodal decomposition and the typical wavelength at which this occurs are well described by the eigenvalue spectrum of the linear theory. In fact the Boltzmann equation for the above lattice gas provides a microscopic model that leads to the phenomenological Cahn-Hilliard equation for spinodal decomposition [13].

After this summary of the information that is contained in the spectra of soft modes, we give the plan of the paper. In Sec. II the eigenvalue problem is formulated. Section III describes the numerical study of spectra and its implications, such as generalized hydrodynamics, thermal effects, and isotropy. Analytic studies of the spectrum in the long- and short-wavelength limit and the consequences of symmetries are discussed in Sec. IV. A discussion of the most salient features is given in Sec. V.

II. EIGENVALUE PROBLEM

The eigenvalue problem studied in this paper is based on the Boltzmann equation, where correlations between time dependent fluctuations are neglected. In formulating the problem we follow essentially the presentation of Refs. [2,14] and generalize the theory to multispeed lattice gases, as is necessary for a discussion of thermal models [15,16]. The average occupation $f(\mathbf{r}, \mathbf{c}_i, t)$ of a state $(\mathbf{r}, \mathbf{c}_i)$ satisfies the nonlinear lattice Boltzmann equation,

$$f(\mathbf{r} + \mathbf{c}_i, \mathbf{c}_i, t + 1) = f(\mathbf{r}, \mathbf{c}_i, t) + I_i(f(t)), \qquad (1)$$

where $i = (1, 2, \ldots, b)$ labels the velocity channels of a b-bit model, and $I_i(f)$ represents the nonlinear collision term, accounting for gains and losses in the f's. The stationary solution of this equation, $f(\mathbf{r}, \mathbf{c}_j, \infty) = f_j^0$ with

$I_i(f^0) = 0$, is the equilibrium distribution, and we restrict ourselves to basic equilibria where the total momentum vanishes and the fluid is macroscopically at rest. In *athermal* lattice gases with only conservation of total momentum and particle number, the stationary distribution is $f_j^0 \equiv f = \rho/b$, where the density ρ is the average number of particles per site. In *thermal* models, where total momentum, particle number and energy are conserved, the stationary distribution is the Fermi distribution,

$$f_j^0 = 1/[1 + \exp(-\alpha + \beta\epsilon_j)]. \tag{2}$$

Here $\epsilon = \frac{1}{2}c_j^2$ is the kinetic energy, α and β are the chemical potential and reciprocal temperature, and $\rho = \sum_j f_j^0$ the density.

The equation for the linear excitation $\delta f_i(\mathbf{r}, \mathbf{c}_i, t) = f(\mathbf{r}, \mathbf{c}_i, t) - f_i^0$ is obtained by linearizing the collision operator I_i around the stationary solution f_i^0, i.e., $I_i(f^0 + \delta f) = \Omega_{ij}\delta f_j + O(\delta f^2)$, where summation convention has been used. The fluctuation at wave number $\mathbf{k}$, introduced in the preceding section, satisfies the basic eigenvalue equation

$$\left[e^{z_\lambda(\mathbf{k}) + i\mathbf{k}\cdot\mathbf{c}} - 1 - \Omega\right] \kappa\psi_\lambda(\mathbf{k}, \mathbf{c}) = 0 \tag{3}$$

in matrix notation. Here $\psi_\lambda(\mathbf{k}, \mathbf{c})$ is a b vector with components $\psi_\lambda(\mathbf{k}, \mathbf{c}_j)$ $(j = 1, 2, \ldots, b)$ and Ω, κ and $\exp(i\mathbf{k}\cdot\mathbf{c})$ are $b \times b$ matrices. The last two are diagonal, i.e., $\kappa_{ij} = \kappa_i\delta_{ij} = f_i^0(1 - f_i^0)\delta_{ij}$ and $[\exp i\mathbf{k}\cdot\mathbf{c}]_{ij} = \delta_{ij}\exp(i\mathbf{k}\cdot\mathbf{c}_j)$. The linearized collision operator can be expressed in terms of the basic transition probabilities that define the collision rules of the lattice gas [6]. If the model satisfies the detailed balance condition, then the symmetry $\Omega_{ij}\kappa_j = \kappa_i\Omega_{ij}$ (no summation) holds. An asymmetric case is treated in Ref. [12]. Here we restrict ourselves to symmetric cases. The eigenmodes of (1) are defined through

$$\begin{aligned}\kappa\psi_\lambda(\mathbf{k}, \mathbf{c}, t) &= \left[e^{-i\mathbf{k}\cdot\mathbf{c}}(1 + \Omega)\right]^t \kappa\psi_\lambda(\mathbf{k}, \mathbf{c}) \\ &= \exp[z_\lambda(\mathbf{k})t]\kappa\psi_\lambda(\mathbf{k}, \mathbf{c}).\end{aligned} \tag{4}$$

The $b \times b$ matrix Ω_{ij} can be calculated analytically or numerically from its definition in terms of the collision rules for the model [6].

In an *athermal* model the collision matrix Ω and its eigenvalues depend only on the density. In a *thermal* model they depend both on density and temperature. Once Ω is known, the eigenvalues of the matrix (3) can be calculated numerically as a function of the wave number $\mathbf{k}$ and the thermodynamic parameters.

The periodic lattice $\mathcal{L}$, upon which the lattice gas is defined, induces symmetries in the eigenvalue spectrum $z_\lambda(\mathbf{k})$ and implies that $\mathbf{k}$ can be restricted to the first Brillouin zone of the reciprocal lattice $\mathcal{L}^*$ with sites $\mathbf{Q} = 2\pi(N_1\boldsymbol{\theta}_1 + N_2\boldsymbol{\theta}_2 + \cdots)$ with $N_1, N_2, \ldots$ integers, because $z_\lambda(\mathbf{k})$ is a periodic function $z_\lambda(\mathbf{k} + \mathbf{Q}) = z_\lambda(\mathbf{k})$. It has all symmetries of the reciprocal lattice $\mathcal{L}^*$, such as inversion symmetry $z_\lambda(\mathbf{k}) = z_\lambda(-\mathbf{k})$. If $\mathcal{L}$ is the triangular lattice with basis or nearest-neighbor lattice vectors $\mathbf{c}_j = (\cos[(j-1)\pi/3], \sin[(j-1)\pi/3])$ with $j = 1, 2, \ldots 6$, then $\mathcal{L}^*$ is the hexagonal lattice, as illustrated in Fig. 1,

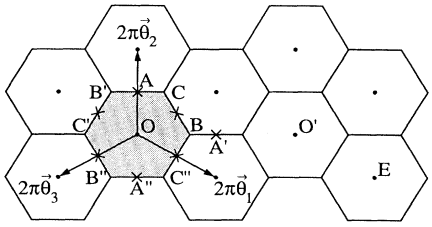

FIG. 1. Wigner-Seitz cell of the reciprocal hexagonal lattice with primitive vectors $2\pi\boldsymbol{\theta}_i$ $(i$=1,2,3), where $\theta_{1,3} = (\pm 1, 1/\sqrt{3})$ and $\theta_2 = (0, 2/\sqrt{3})$.

with basis vectors $2\pi\boldsymbol{\theta}_j$ satisfying $\boldsymbol{\theta}_\ell \cdot \mathbf{c}_j = -1$, 0, or 1. The first Brillouin zone is the Wigner-Seitz cell (shaded in Fig. 1) of $\mathcal{L}^*$.

In the next section we present the numerical results for the spectra. We analyze their properties and study their implications. Section IV deals with analytical calculations.

III. STRUCTURE OF SPECTRA

The numerical problem is rather simple. It involves the calculation of the b roots of the secular determinant of the complex matrix in (3) as a function of the reciprocal lattice vector $\mathbf{k}$. The eigenvalues $z_\lambda(\mathbf{k}) = \mathrm{Re}\, z_\lambda(\mathbf{k}) + i\,\mathrm{Im}\, z_\lambda(\mathbf{k})$ are in general complex, and $\mathrm{Im}\, z_\lambda(\mathbf{k})$ is defined mod 2π. We first consider a two-dimensional lattice gas, defined on a triangular lattice, that involves one rest particle with velocity $\mathbf{c}_0 = \mathbf{0}$ and six moving particles with velocities $\mathbf{c}_j$ $(j = 1, \ldots, 6)$ equal to the nearest-neighbor lattice vectors. The model is referred to as the seven-bit FHP-III lattice gas, named after Frisch, Hasslacher, and Pomeau [6], and its detailed collision rules are listed Ref. [7]. The resulting dispersion relations are shown in Fig. 2, where parts (a) and (b) show the real and imaginary parts of all seven eigenvalues in the direction of highest symmetry, i.e., $\mathbf{k}$ parallel to the y axis. Parts (c) and (d) refer to the perpendicular direction with $\mathbf{k}$ parallel to the x axis. Inspection of Fig. 1 shows that the periods in those two directions are $4\pi/\sqrt{3}$ and 4π, respectively. There are several interesting features to be discussed.

A. Hydrodynamic regime

The spectrum of Fig. 2 shows three soft hydrodynamic modes, with $\mathrm{Re}\, z_\mu(0) = 0$, labeled $\{\perp, \pm\}$, and four hard kinetic modes with $\mathrm{Re}\, z_\lambda(0) < 0$, labeled $\{4, 5, 6, 7\}$. The hydrodynamic modes consist of two propagating damped *sound* modes $(\lambda = \pm)$ with $\mathrm{Im}\, z_\pm(\mathbf{k}) = \mp c(\mathbf{k})k \neq 0$ and one diffusive *transverse momentum* (*shear*) mode $(\lambda = \perp)$ with $\mathrm{Im}\, z_\perp(\mathbf{k}) = 0$. The real parts of $z_\pm(\mathbf{k})$ coincide and are shown as the lower branch in Figs. 2(a) and 2(c). The real parts of hydrodynamic and kinetic eigenvalues are well separated for $k < k_1$, where k_1 is the wave number

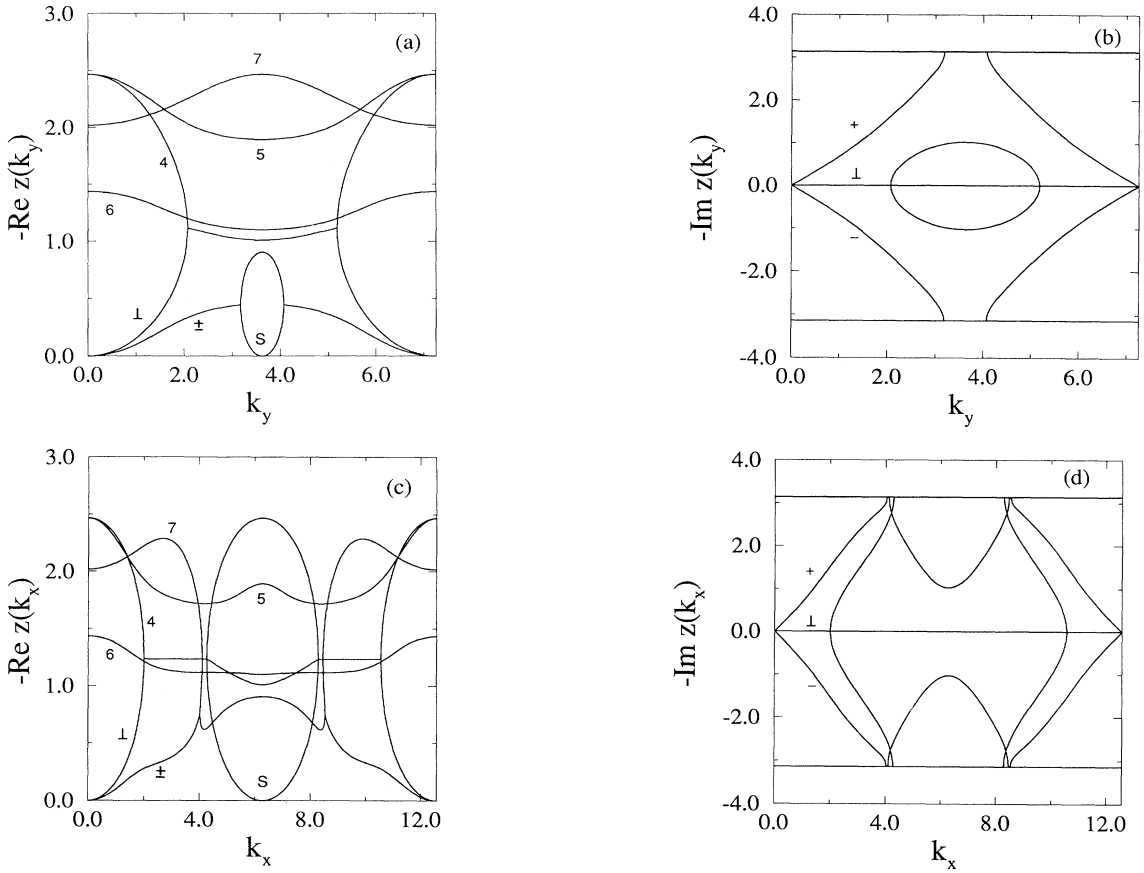

FIG. 2. Real and imaginary part of the spectrum $z_\lambda(\mathbf{k})$, for the seven-bit FHP-III model at density $\rho = 1.4$, with (a) and (b) $\mathbf{k} = (0, k)$ and (c) and (d) $\mathbf{k} = (k, 0)$. The labels refer to the "soft" shear ($\perp$) and sound ($\pm$) modes, the staggered modes (s), and the "hard" kinetic $(4, 5, 6, 7)$ modes.

at which for the first time a hydrodynamic and kinetic eigenvalue are equal. Wave numbers on the order of k_1 characterize the kinetic regime. In Fig. 2, where the density $\rho = 1.4$, one has $k_1 \simeq 2.1$. In a closely related lattice gas with six velocity states $\mathbf{c}_i$ per node, and referred to as the athermal six-bit FHP-I model in Ref. [7], the kinetic regime starts at much smaller wave numbers. One has, for instance, $k_1 \simeq 0.4$ at $\rho = 1.2$.

In the limit of small k (actually $k\ell_0 \ll 1$ where ℓ_0 is the mean free path) the eigenvalues are given by the hydrodynamic dispersion relations

$$z_\pm(\mathbf{k}) = \mp ic_s k - \Gamma k^2, \quad z_\perp(\mathbf{k}) = -\nu k^2, \tag{5}$$

where c_s is the speed of sound, ν is the shear viscosity, and Γ is the sound damping constant, given in athermal models by $\Gamma = \frac{1}{2}(\nu+\zeta)$ with ζ the bulk viscosity. Because of periodicity the same behavior pertains around every site $\mathbf{Q}$ of the reciprocal lattice, with $|\mathbf{k}|$ in (5) replaced by $|\mathbf{k} - \mathbf{Q}|$.

B. Generalized hydrodynamics

When $\mathbf{k}$ increases, the dispersion relations of classical hydrodynamics with $\mathbf{k}$-independent transport coefficients break down and we enter the regime of generalized hydrodynamics, where the dispersion relations can be represented approximately by (5) with a slowly varying $\mathbf{k}$-dependent speed of sound $c_s(\mathbf{k})$ and $\mathbf{k}$-dependent transport coefficients $\Gamma(\mathbf{k})$ and $\nu(\mathbf{k})$. Inspection of Figs. 2(b) and 2(d) shows that the speed of sound $c_s(\mathbf{k})$ is constant up to $k \simeq 1$. At what $\mathbf{k}$ values do the transport coefficients become $\mathbf{k}$ dependent? To answer that question for the FHP-I model we have plotted the shear viscosity $\nu(\mathbf{k}) \equiv -z_\perp(\mathbf{k})/k^2$ (solid line) and the sound damping constant $\Gamma(\mathbf{k}) \equiv -\mathrm{Re}\, z_\pm(\mathbf{k})/k^2$ (dashed line) as a function of k for three different $\mathbf{k}$ directions in Fig. 3.

In the hydrodynamic regime one has constant transport coefficients by definition. For $k \to 0$ the sound damping constant $\Gamma(\mathbf{k}) \to \Gamma = \frac{1}{2}\nu$ in FHP-I, since the bulk viscosity vanishes in a single speed model. Inspection of Fig. 3 shows that the transport coefficients are approximately constant for $|\mathbf{k}| \leq k_h \simeq 0.1$. Consequently, if one wants to measure the *constant* transport coefficients in computer simulations from the decay of a sinusoidal wave, its wavelength $\lambda = 2\pi/k$ should satisfy $\lambda \geq \lambda_h \simeq 60$ lattice units. For the seven-bit FHP-III model it can be read off from Figs. 2(a) and 2(c) that $k_h \simeq 2$ or $\lambda_h \simeq 3$.

For FHP-III the shear mode mixes at $|\mathbf{k}| = 2.1$ with

a kinetic mode, resulting in two strongly damped propagating modes. This can be seen from Figs. 2(a)–2(d), where two propagating modes appear at $k = 2.1$. Figure 2(b) also shows a propagation gap [Im $z_{\pm}(\mathbf{k}) = \pm\pi$] in the interval $3.2 \leq |\mathbf{k}| \leq 4.1$.

The solid lines in Figs. 3(b) and 3(c) for FHP-I end at a wave number $k_1 \simeq 0.4$, where the shear mode mixes with a kinetic mode and changes its character from a purely diffusive to a propagating mode. For $|\mathbf{k}|$ values larger than k_1, generalized hydrodynamics has lost all meaning, at least with respect to the transverse momentum or shear mode. In Fig. 3(a), where $\mathbf{k} \| \hat{\mathbf{y}}$, the shear mode does not mix with a kinetic mode. Similar propagation gaps of sound modes have been found from the revised Enskog theory for dense hard-sphere systems and have been observed in the dynamic structure factor $S(k, \omega)$ in neutron-scattering experiments on liquid argon and liquid metals [17]. The dispersion relations for a two-dimensional thermal lattice gas, defined on a triangular lattice with 19 different velocity states per node, are discussed in Ref. [15].

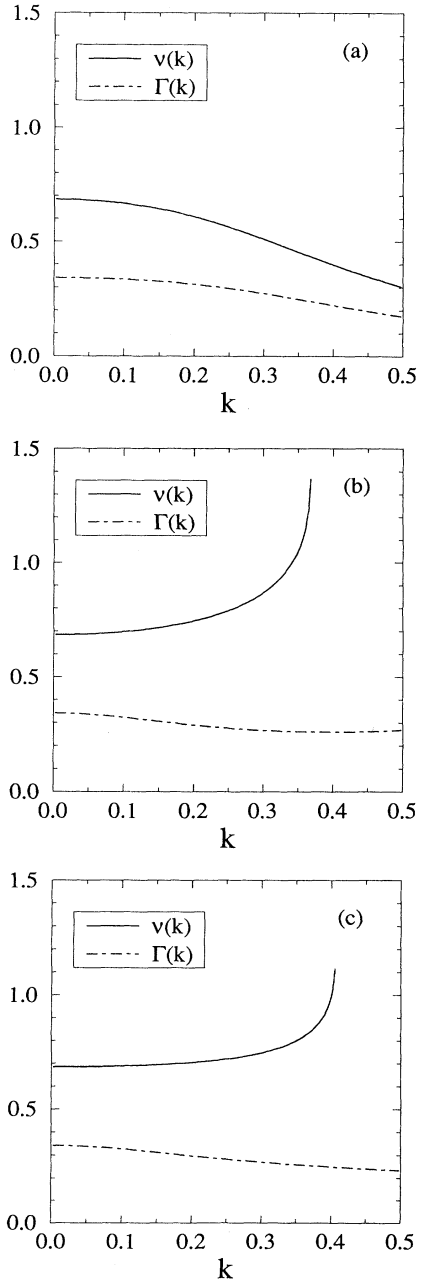

FIG. 3. Shear viscosity $\nu(\mathbf{k})$ and sound damping constant $\Gamma(\mathbf{k})$ vs k, for the six-bit FHP-I model at $\rho = 1.8$, in three different $\mathbf{k}$ directions: (a) $\mathbf{k} \| \hat{\mathbf{y}}$, (b) $\mathbf{k} \| \hat{\mathbf{x}}$, and (c) $\mathbf{k} \| \overrightarrow{OE}$ in Fig. 1.

C. Negative bulk viscosity

The generalized hydrodynamic effects on transport coefficients, shown in Fig. 3, also provide a quantitative explanation for some older puzzling simulation results in the literature [7,8], described as a "negative bulk viscosity." The simulation data for the FHP-I model [7] are shown in Fig. 4 as dots, referring to the shear viscosity, and squares, referring to the sound damping constant.

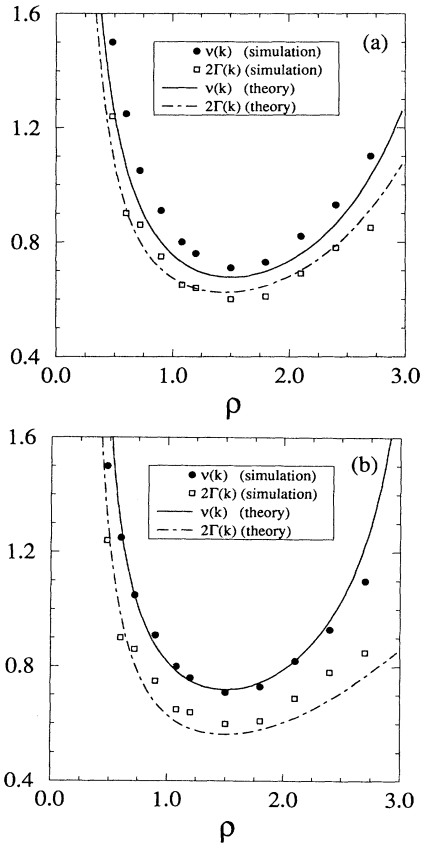

FIG. 4. $\mathbf{k}$ dependent shear viscosity ν and sound damping constant Γ vs density ρ, for the six-bit FHP-I model, with $\mathbf{k} \| \hat{\mathbf{x}}$ and (a) $k = 0.1$ and (b) $k = 0.2$, respectively. The simulation data were taken from Ref. [9]. The graphs show that the $\mathbf{k}$-dependent bulk viscosity $\zeta(\mathbf{k}) = 2\Gamma(\mathbf{k}) - \nu(\mathbf{k})$ is negative for this $\mathbf{k}$ direction.

We assume that these simulations were carried out with a $\mathbf{k}$ vector *parallel* to a lattice vector, as in Fig. 3(b), and not under some angle as in Figs. 3(a) and 3(c), although this information is not provided in Ref. [7]. The computer experiments were carried out at wavelengths between 30 and 80 lattice units, corresponding to $k \simeq 0.2$ and $k \simeq 0.08$, respectively, and the results were averaged over this $\mathbf{k}$ interval. In Fig. 4 the simulation data are compared with the $\mathbf{k}$-dependent shear viscosity $\nu(\mathbf{k})$ (solid line) and the $\mathbf{k}$-dependent sound damping constant $2\Gamma(\mathbf{k})$ (dashed line).

In addition to the (positive) wave-number-dependent damping coefficients $\nu(\mathbf{k})$ and $\Gamma(\mathbf{k})$ one may also introduce a wave-number-dependent bulk viscosity $\zeta(\mathbf{k}) \equiv 2\Gamma(\mathbf{k}) - \nu(\mathbf{k})$ based on the analogous formula $\zeta \equiv 2\Gamma - \nu$, valid in the long-wavelength limit, where $\zeta > 0$ in the FHP-III model and $\zeta = 0$ in the FHP-I model. Inspection of Fig. 3 shows that $\zeta(\mathbf{k})$ is negative for $\mathbf{k} \| \hat{\mathbf{x}}$ [Fig. 3(b)] and positive for $\mathbf{k} \| \hat{\mathbf{y}}$ [Fig. 3(a)] in the range of wave numbers of interest in the simulations. This is confirmed in a more quantitative manner by Figs. 4(a) and 4(b), where the generalized hydrodynamics results at $\mathbf{k} = (0.1, 0)$ and $\mathbf{k} = (0.2, 0)$ are compared with computer simulations, obtained by averaging the simulation data over the k interval $(0.08, 0.2)$. The observation that $2\Gamma_{\text{sim}} < \nu_{\text{sim}}$ [7,8] has been misinterpreted as a negative bulk viscosity. The good agreement between theory and simulations, especially near the large $\mathbf{k}$ end of the averaging interval, convincingly shows that the experiments were done outside the range of classical hydrodynamics. The essential point that explains the large difference between $\nu(\mathbf{k})$ and $2\Gamma(\mathbf{k})$ in Fig. 4 is that the two curves in Fig. 3(b) move away from each other with increasing k. Suppose one would do computer experiments in a $\mathbf{k}$ direction making an angle of 30° with a lattice vector, as in Fig. 3(a). On the basis of the same arguments it would then follow that possible simulation data for $\nu_{\text{sim}}(\mathbf{k})$ and $2\Gamma_{\text{sim}}(\mathbf{k})$ would almost coincide, but the inequality would be reversed. In Ref. [8] another simulation result on negative bulk viscosity is reported, also for a six-bit triangular lattice gas with collision rules slightly different from FHP-I. The $\mathbf{k}$ values used in the computer experiments are not listed, so that a quantitative comparison with the theory is not possible. We stress that the negative bulk viscosity effect is not a finite-size effect. It also occurs on an infinite lattice at the same $\mathbf{k}$ vector.

D. Thermal effects

The simplest thermal lattice gas is a nine-bit model, defined on a square lattice, with four speed-1, four speed-$\sqrt{2}$ particles, and one rest particle. It is discussed in [18,19]. Figure 5 shows the hydrodynamic part of the spectrum $z_\lambda(\mathbf{k})$ with $\mathbf{k} \| \hat{\mathbf{x}}$ or $\hat{\mathbf{y}}$, for this lattice-gas model. The five kinetic eigenvalues (not shown) can become as large as 4.8 for small k. In thermal models energy is conserved. This leads to an additional hydrodynamic mode, the heat mode, labeled $\lambda = T$, with a dispersion relation for $\mathbf{k} \to \mathbf{0}$,

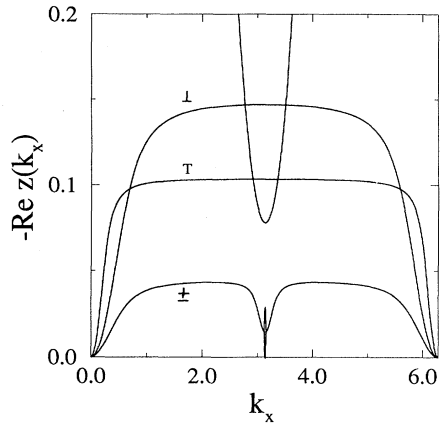

FIG. 5. Hydrodynamic part of the spectrum $z_\lambda(\mathbf{k})$, with $\mathbf{k} \| (1,0)$, for the nine-bit thermal square lattice gas of Ref. [19,20] at $e^\alpha = 0.8$ and $e^\beta = 0.64$, yielding $\rho = 3.36$. The labels refer to the shear ($\perp$), heat (T), and sound ($\pm$) modes.

$$z_T(\mathbf{k}) = -D_T k^2, \tag{6}$$

where D_T is the thermal diffusivity. Inspection of Fig. 5 shows the existence of four hydrodynamic modes. The lowest branch at small k represents the two sound mode eigenvalues $z_\pm(\mathbf{k})$, the middle branch the shear mode eigenvalue $z_\perp(\mathbf{k})$, and the top branch the heat mode eigenvalue $z_T(\mathbf{k})$. Around $\mathbf{k} = (\pi, 0)$ one of the kinetic eigenvalues becomes smaller than 0.2. Also close to $\mathbf{k} = (\pi, 0)$ the two propagating sound modes change into a pair of slow diffusive modes (see Sec. III F on spurious soft modes). For $k < 2.7$ the real parts of hydrodynamic and kinetic eigenvalues are well separated. However, the $\mathbf{k}$ range for which standard hydrodynamics holds is extremely small, as is shown in Fig. 6 for the $\mathbf{k}$-dependent viscosity $\nu(\mathbf{k})$ and in Fig. 7 for the $\mathbf{k}$-dependent heat diffusivity $D_T(\mathbf{k}) \equiv -z_T(\mathbf{k})/k^2$. Both figures are extracted from Fig. 5. Generalized hydrodynamic effects are particularly strong in Fig. 7, where $D_T(\mathbf{k})$ is only constant for $\lambda = 2\pi/k > \lambda_h \simeq 50$ lattice units. For $\lambda < \lambda_h$

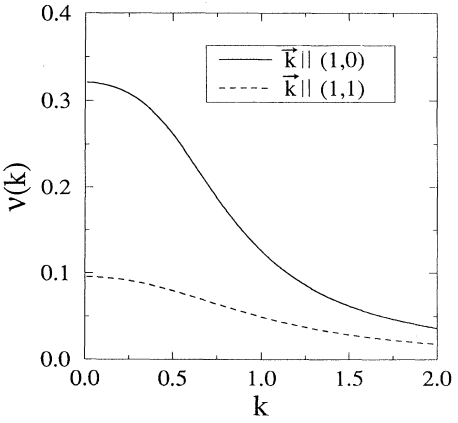

FIG. 6. Viscosity $\nu(\mathbf{k})$ vs k, for the model of Fig. 5, with $\mathbf{k} \| (1,0)$ (solid line) and $\mathbf{k} \| (1,1)$ (dashed line).

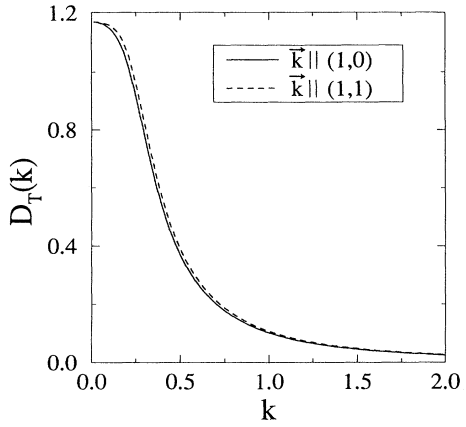

FIG. 7. Heat diffusivity $D_T(\mathbf{k})$ vs k, for the model of Fig. 5, with $\mathbf{k}\|(1,0)$ (solid line) and $\mathbf{k}\|(1,1)$ (dashed line).

the heat diffusivity $D_T(\mathbf{k})$ rapidly falls off by an order of magnitude. For the shear viscosity the effects of generalized hydrodynamics are less pronounced and become only noticeable for $\lambda < 25$.

In conclusion, the nine-bit model, apart from being anisotropic, as discussed in Sec. III E, is not suitable to study Fourier's heat law with constant transport coefficients. The relation between the heat flux and the temperature gradient is strongly nonlocal, extending over a distance $\lambda_h \simeq 50$, as compared to $\lambda_h \simeq 3$ in the FHP-III model. In simulations of the nine-bit square lattice gas one would need a system size a factor $(50/3)^2$ larger than in FHP-III to have an equivalent range of k values where standard hydrodynamic behavior holds.

E. Isotropy

The isotropy of the spectrum of the FHP-III lattice gas at small k is due to the hexagonal symmetry of the triangular lattice underlying these models. In Fig. 2 the real and imaginary parts of $z_\lambda(\mathbf{k})$ are approximately independent of the direction of $\mathbf{k}$ for small k. At larger k values the isotropy breaks down for all lattices. With decreasing density the isotropy breaks down at smaller and smaller k values. The pronounced difference between the results for the different $\mathbf{k}$ directions in Fig. 4, as discussed in Sec. III B on generalized hydrodynamics, is another illustration of anisotropic effects in lattice gases.

On square lattices the spectrum is anisotropic even on the longest wavelengths, as shown in Fig. 6 for the decay rate $z_\perp(\mathbf{k})$ of the shear mode. This quantity can be expressed in terms of the $(\perp\ell\perp\ell)$ element of the fourth-rank viscosity tensor $\nu_{\alpha\beta\gamma\delta}$, where ℓ refers to longitudinal and $\perp$ to transverse components with respect to $\mathbf{k}$. On a square lattice this tensor is not isotropic and contains in principle three different types of scalar viscosities ν, ϑ, and ζ ($\zeta = 0$ in the nine-bit square lattice gas), as discussed in Ref. [19]. From that reference one readily derives the angular dependence of the damping constant of the shear mode as $|\mathbf{k}| \to 0$. The result is

$$\nu(\mathbf{k}) = \nu_{\perp\ell\perp\ell}(\hat{k}) = \nu\cos^2\phi + \vartheta\sin^2\phi, \tag{7}$$

where $\cos(\frac{1}{2}\phi) = \hat{\mathbf{k}}_x$ is the x component of the unit vector $\hat{\mathbf{k}} = \mathbf{k}/|\mathbf{k}|$. The solid line in Fig. 6 refers to $\mathbf{k}$ along the $\hat{\mathbf{x}}$ axis ($\phi = 0$) and the dashed line to $\mathbf{k}$ along the main diagonal ($\frac{1}{2}\phi = \frac{1}{4}\pi$).

F. Spurious soft modes

Another conspicuous feature in the spectra $z_\lambda(\mathbf{k})$ is the occurrence of a soft mode at $\mathbf{k} = (0, 2\pi/\sqrt{3})$ in Fig. 2(a) and at $\mathbf{k} = (2\pi, 0)$ in Fig. 2(c). These soft modes are the well-known staggered momentum densities [3]. They occur at the centers of the faces of the first Brillouin zone (A, A', A'' and equivalent points in Fig. 1). In the vicinity of the point A the spectrum can be represented by [14]

$$z_\theta(\mathbf{k}) = -\{D_\| \cos^2\chi + D_\perp \sin^2\chi\}\,|\mathbf{k} - \pi\boldsymbol{\theta}|^2 \tag{8}$$

with $\cos\chi = \hat{\mathbf{k}}\cdot\hat{\boldsymbol{\theta}}$. Carets denote unit vectors. The staggered diffusivity is not isotropic and can be decomposed into a longitudinal ($D_\|$) and a transverse ($D_\perp$) diffusivity. For $\mathbf{k} = (0, k_y)$ [see Fig. 2(a)] and $\mathbf{k} = (k_x, 0)$ [see Fig. 2(c)] it reduces to

$$\begin{aligned} z_\theta(k_y) &= -D_\| \left(k_y - \frac{2\pi}{\sqrt{3}}\right)^2, \\ z_\theta(k_x) &= -D_\perp (k_x - 2\pi)^2. \end{aligned} \tag{9}$$

In Fig. 5 a similar staggered momentum mode can be observed at $\mathbf{k} = (\pi, 0)$ and $\mathbf{k} = (0, \pi)$. The corresponding diffusivities have been calculated in Refs. [3,20] for six- and seven-bit athermal triangular lattice gases and in Ref. [19] for the thermal nine-bit lattice gas. In all models $D_\perp = \nu$, on the basis of lattice symmetries, as will be shown in Sec. IV C. This can also be seen in Fig. 2(c) by comparing the curvature of the soft modes at $k = 0$ and $k = 2\pi/\sqrt{3}$. The longitudinal diffusivity $D_\|$ has in general *no* relationship to either shear or bulk viscosity [note the difference in curvature between the soft modes at $k = 0$ and $k = 2\pi$ in Fig. 2(a)].

IV. ANALYTIC RESULTS

A. Hydrodynamic regime

One of the main interests of lattice gases is their applicability for simulating nonequilibrium fluids. Hence the most interesting part of the spectrum is the hydrodynamic part with phenomena varying on spatial scales large compared to the lattice distance and large compared to the mean free path. By setting first $\mathbf{k} = 0$ in (3) we obtain

$$(1 + \Omega)\kappa u_n = \exp[z_n(0)]\kappa u_n \equiv (1 - \omega_n)\kappa u_n, \tag{10}$$

where $-\omega_n$ ($\omega_n \geq 0$) are the eigenvalues of the linearized collision operator. The $(d + 2)$ collisional invariants for a d-dimensional thermal lattice gas are the zero eigen-

vectors ($\omega_n = 0$), with $u_n(\mathbf{c}) = \{1, c_x, c_y, \ldots, c_d, \frac{1}{2}c^2\}$. In athermal models $\frac{1}{2}c^2$ is excluded from this set since energy is not conserved. The remaining kinetic eigenvalues obey $0 < \omega_n < 2$, where ω_n is explicitly known for the majority of thermal and athermal lattice gases [15,19,20]. In FHP-I all eigenvalues satisfy the inequality $\omega_n < 1$. In FHP-III some ω_n's do exceed unity, and $z_n(0) = \pi i + \ln|\omega_n - 1| + \mathrm{mod}(2\pi i)$. This can be seen in Fig. 2 where $\mathrm{Im}\, z_6(0) = -\pi$ and $\mathrm{Re}\, z_6(0) \simeq 2.0$. Furthermore, the twofold-degenerate kinetic eigenvalue with $\mathrm{Re}\, z_{4,5}(0) \simeq 2.5$ corresponds to $\omega_{4,5} = \omega_\nu$, which is directly related to the shear viscosity ν, as we shall see below.

For a further analysis of the spectrum we need the explicit form of the eigenfunctions $u_n(\mathbf{c})$, defined by $\Omega\kappa u_n = -\omega_n \kappa u_n$. In athermal models the factor κ can be dropped, because $\kappa_{ij} = f(1-f)\delta_{ij}$, with $f = \rho/b$, is simply a multiple of the unit matrix. The simplest nontrivial examples are again the six- and seven-bit triangular lattice gases, where the eigenfunctions are b vectors ($b = 6, 7$) with components $u_n(\mathbf{c}_j)$, with $j = 1, 2, \ldots 6$, for six-bit models and $j = 0, 1, 2, \ldots, 6$ for seven-bit models with $\mathbf{c}_0 = \mathbf{0}$. They are given in Table I, which has been taken from Ref. [20]. For the thermal nine-bit square lattice gas similar tables have been constructed [19]. In Fig. 2 the kinetic eigenvalues at small $\mathbf{k}$ values are labeled with the labels $n = 4, 5, 6, 7$ of the corresponding eigenfunctions u_n in Table I.

The eigenfunction $u_n(\mathbf{c})$ can be used as a starting point for determining the eigenfunctions and eigenvalues of (3) as a Taylor series expansion in a small parameter k, or more precisely $k\ell_0$. The dimensionless parameter satisfies $k\ell_0 \ll 1$, implying that the relevant wavelengths are large compared to the mean free path ℓ_0. In the kinetic regime $k\ell_0$ is of order unity and in the free-particle regime $k\ell_0 \gg 1$. In the free-particle regime, to be discussed in Sec. IV B, perturbation expansions will be based on the small parameter $1/(k\ell_0)$.

In the hydrodynamic regime one writes for the soft modes

$$z_\lambda(\mathbf{k}) = ikz_\lambda^{(1)} + (ik)^2 z_\lambda^{(2)} + \cdots, \qquad \psi_\lambda(\mathbf{k}, \mathbf{c}) = \psi_\lambda^{(0)}(\mathbf{c}) + \cdots . \tag{11}$$

TABLE I. Eigenfunctions $u_n(\mathbf{c})$ and eigenvalues ω_n of (10) for the six- and seven-bit FHP models and parity of $u_n(\mathbf{c})$ under reflections. The eigenvalues ω_ν (twofold degenerate), ω_g and ω_ζ are given in Ref. [14]. c_s is the speed of sound.

n	$u_n(\mathbf{c})$	ω_n	Parity $x \leftrightarrow -x$	Parity $y \leftrightarrow -y$
1	1	0	+	+
2	c_x	0	−	+
3	c_y	0	+	−
4	$c_x c_y$	ω_ν	−	−
5	$c_x^2 - c_y^2$	ω_ν	+	+
6	$(4c_x^2 - 3)c_x$	ω_g	−	+
7	$\frac{1}{2}c^2 - c_s^2$	ω_ζ	+	+

This can be done by using degenerate perturbation theory. For continuous gases the method is described in Ref. [21]. Some technical complications in lattice gases, resulting from the discreteness of space, time and velocity variables, are discussed in [2,14]. The extension to thermal models is straightforward [15]. Perturbation theory yields hydrodynamic dispersion relations in agreement with (5) together with explicit expressions for the sound damping constant $\Gamma = \frac{1}{2}(\nu + \zeta)$, kinematic viscosity ν, and bulk viscosity ζ. For the FHP-I and FHP-III models these values are listed in Ref. [7]. In the long-wavelength limit the hydrodynamic modes are found as linear combinations of the collisional invariants, yielding to zeroth order in the expansion parameter k

$$\begin{aligned} \psi_\pm^{(0)}(\mathbf{c}) &= \begin{cases} c_s \pm \mathbf{c}\cdot\hat{\mathbf{k}} & \text{(athermal)} \\ \frac{1}{2}c^2 \pm c_s \mathbf{c}\cdot\hat{\mathbf{k}} & \text{(thermal)}, \end{cases} \\ \psi_\perp^{(0)}(\mathbf{c}) &= \mathbf{c}\cdot\hat{\mathbf{k}}_\perp, \\ \psi_T^{(0)}(\mathbf{c}) &= \tfrac{1}{2}c^2 - c_s^2 \quad \text{(thermal only)}\ , \end{aligned} \tag{12}$$

where $\hat{\mathbf{k}}$ and $\hat{\mathbf{k}}_\perp$ are unit vectors, parallel and perpendicular to $\mathbf{k}$, respectively. The (adiabatic) speed of sound c_s is given by

$$c_s^2 = \frac{dp}{d\rho} = \begin{cases} \sum_i c_i^2/db & \text{(athermal)} \\ \frac{1}{2}\sum_i \kappa_i c_i^4 \Big/ \sum_i \kappa_i c_i^2 & \text{(thermal)} \end{cases} \tag{13}$$

with $\kappa_i = f_i^0(1 - f_i^0)$.

B. Free-particle regime

In the kinetic regime, where $k\ell_0 \simeq 1$, perturbation methods cannot be used. However, in the free-particle regime, where $1/(k\ell_0)$ is a small parameter, analytic results for the spectra can again be obtained perturbatively. The fewer the number of (binary, triple, quadruple, etc.) collisions, the sooner the eigenvalue spectrum of (3) crosses over from the hydrodynamic spectrum to a free-particle spectrum, where the effect of the collision matrix Ω is only a small perturbation on the propagating part of the operator in Eq. (3). A reduction of the collision frequency and increase of the mean free path is not only realized by reducing the density, but also by considering models with very few active collisions. This effect can be seen by comparing the plots in Figs. 2 and 8. They show the spectrum of the seven-bit FHP-III model, where ten collisions are active [7], and that of the six-bit FHP-I model, where there are only two active collisions (binary and triple collisions with a vanishing total momentum). It is therefore expected that the features of the free-particle spectra are more dominant in FHP-I, as illustrated in Fig. 8.

Before commenting on these numerical results we consider the eigenvalue equation (3) for small densities ($\rho =$

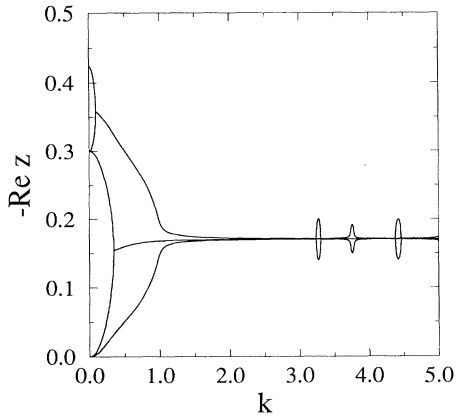

FIG. 8. Real part of the spectrum $z_\lambda(\mathbf{k})$, for the six-bit FHP-I model at $\rho = 2.4$, vs k for $\mathbf{k} \| \overrightarrow{OE}$ in Fig. 1.

$bf \to 0$). At $f = 0$ (free-particle case) the eigenvalues and eigenmodes for the FHP-I model are

$$z_\lambda^0(\mathbf{k}) = -i\mathbf{k}\cdot\mathbf{c}_\lambda \quad (\lambda = 1,2,\ldots,6),$$
$$\psi_\lambda^0(\mathbf{c}_j) = \delta_{\lambda j} \quad (j = 1,2,\ldots,6), \tag{14}$$

where λ labels the eigenmodes and j the components of the six vectors $\psi_\lambda(\mathbf{c})$. The superscript (0) refers to vanishing density, i.e., all six modes are propagating. For small densities and general $\mathbf{k}$ vectors (differing from the special directions $\overrightarrow{OA}$ and $\overrightarrow{OA'}$ of highest symmetry in Fig. 1) first-order perturbation theory yields

$$z_\lambda(\mathbf{k}) = -i\mathbf{k}\cdot\mathbf{c}_\lambda + \Omega_{\lambda\lambda}. \tag{15}$$

The matrix elements of the circulant matrix Ω_{ij} only depend on $|i-j|$, and straightforward calculation yields that $\Omega_{\lambda\lambda} = -f(1-f)^2$, independent of λ. Therefore $\mathrm{Re}\, z_\lambda(\mathbf{k}) = f(1-f)^2$ is sixfold degenerate. Minor modifications yield for FHP-III at low densities $\Omega_{\lambda\lambda} \simeq -4f$ ($\lambda = 1,2,\ldots,6$) and $\Omega_{00} \simeq -6f$, where $\lambda = 0$ refers to the rest particle state. This yields, instead of (15), six propagating modes with $\mathrm{Re}\, z_\lambda(\mathbf{k}) \simeq -4f$ with a sixfold degeneracy, and one nonpropagating mode with $z_0(\mathbf{k}) \simeq -6f$. Figure 8 shows an FHP-I spectrum in a low-symmetry $\mathbf{k}$ direction. Perturbation results are in good agreement with the analytical results for all $|\mathbf{k}| > 1$. For $\mathbf{k}$ in directions of high symmetry, for instance, parallel to the x or y axis, the eigenvalues at large k values can be calculated by first-order perturbation theory for degenerate levels. One finds slightly different results, which also agree very well with the numerical evaluation.

The perturbation results for the free-particle regime in the model FHP-III are only observed for densities $f \leq 0.05$. However, the FHP-I spectra show strong free-particle features at all densities, as can be seen from Fig. 8 ($f = 0.4$) for the real parts of the eigenvalues. One observes a narrow hydrodynamic regime ($k \leq 0.1$; see also Fig. 3) and a subsequent generalized hydrodynamic regime, after which the spectra rapidly cross over to typical free-particle features at $k \geq 1$, with a wave-number-independent damping of propagating modes. The predicted eigenvalues in (15), based on first-order perturbation theory, are quantitatively correct for all densities within a few percent. The propagation speeds $\{\frac{1}{2}\sqrt{3}, \frac{1}{2}, 1\}$ of the modes are in very good agreement with the free-particle predictions for all densities in the whole Brillouin zone, except for a very small hydrodynamic region around $k = 0$, where two propagating sound modes with speed $c_s = 1/\sqrt{2}$, one soft shear mode, and three nonpropagating kinetic modes are observed.

In recent simulations on the FHP-I model, carried out by Grosfils, Boon, and Lallemand [22], the dynamic structure factor $S(\mathbf{k},\omega)$ was measured at a reduced density $\rho = 2.33$, for wave vectors in different directions and with magnitudes k ranging from 0.07 to 0.7. These wave numbers extend well into the regime of generalized hydrodynamics. The authors observed a Brillouin doublet, located approximately at $\Delta\omega \simeq \pm c_s k$ with $c_s \simeq 1/\sqrt{2}$. The width of the Brillouin lines is given by $-\mathrm{Re}\, z_\pm(\mathbf{k}) = \Gamma(k)k^2$ with a k-dependent sound damping constant, which was parametrized as

$$-\mathrm{Re}\, z_\pm(\mathbf{k}) = k^2\Gamma(k) = \Gamma k^2/(1 + k^2\xi^2). \tag{16}$$

We compare this formula with the curve for $-\mathrm{Re}\, z_\pm(\mathbf{k})$ in Fig. 8 (smallest eigenvalue at small k). For large $|\mathbf{k}|$, the quantity $k^2\Gamma(\infty) \simeq \Gamma/\xi^2$ can be estimated as $|\Omega_{11}| = f(1-f)^2$ on the basis of (15) for arbitrary $\mathbf{k}$ directions. The simulation value in Ref. [22], $\Gamma(0) = 0.313$, is roughly in agreement with the theoretical prediction $\Gamma = \frac{1}{2}\nu = 0.440$; the measured correlation length [22], $\xi_{\mathrm{sim}} \simeq 4.6$, is in the right order of magnitude of the theoretical estimate, $\xi_{\mathrm{theor}} \simeq 1.7$ at this density.

C. Symmetries of spectra

The two preceding subsections are based on perturbation theory. Of great help in analyzing eigenvalue problems are the symmetry operations that leave the matrix in (3) invariant. Of course the $\mathbf{k}$ vector in (3) destroys most of the lattice symmetries of the collision matrix Ω_{ij} that is invariant under all symmetries of the discrete space group of the underlying lattice.

For general $\mathbf{k}$ directions the matrix in (3) has no special symmetries. However, if $\mathbf{k}$ is parallel to the x axis, the matrix depends only on $\exp(ikc_x)$ and the full matrix is then invariant under reflection $y \Leftrightarrow -y$. Similar observations hold for $\mathbf{k}$ parallel to the y axis. On a triangular lattice these two invariances are distinct, on the square lattice they are not. Concentrating on the FHP models, we can therefore decompose the b-dimensional basis ($b =$ 6 or 7) of $u_n(\mathbf{c})$ in Table I into a two-dimensional subspace of odd parity under the reflection $y \Leftrightarrow -y$, spanned by the eigenvectors $u_3(\mathbf{c})$ and $u_4(\mathbf{c})$, and into a four-dimensional ($b = 6$) or five-dimensional subspace ($b = 7$) of even parity, spanned by the remaining eigenvectors $u_n(\mathbf{c})$. Therefore the matrix (3) with $\mathbf{k} = (k,0)$ has a block-diagonal form as all matrix elements connecting the odd and even subspaces vanish [2]. The (3,4) block

is of odd parity, where $\mathbf{k} = (k, 0)$ has the eigenvalues

$$\begin{aligned}\exp[z_{3,4}(\mathbf{k})] &= \Lambda_{3,4}(k) \\ &= (1 - \tfrac{1}{2}\omega_\nu)\cos(\tfrac{1}{2}k) \\ &\quad \pm[(1 - \tfrac{1}{2}\omega_\nu)^2 \cos^2(\tfrac{1}{2}k) - 1 + \omega_\nu]^{1/2},\end{aligned} \tag{17}$$

implying the relation $\Lambda_{3,4}(k + 2\pi) = -\Lambda_{4,3}(k)$. Consequently, Re $z_{3,4}(k + 2\pi) =$ Re $z_{4,3}(k)$ are simply shifted by an amount 2π. This symmetry also shows that the diffusivities ν and $D_\perp$ in Fig. 2(c) of the shear mode $z_\perp(\mathbf{k}) = -\nu k^2$ and the staggered mode $z_\theta(\mathbf{k}) = -D_\perp(k - 2\pi)^2$ are necessarily equal. The shift symmetry is absent in Fig. 2(a), where $\mathbf{k} = (0, k)$. It is also easy to verify that Eq. (17) explains the horizontal parts in Re$z_{3,4}(k)$ for $2 \lesssim k \lesssim 4$ and $8.5 \lesssim k \lesssim 10.5$ in Fig. 2(c).

In the case $\mathbf{k} = (0, k)$ the matrix (3) for FHP models is invariant under the reflection $x \Leftrightarrow -x$, and Table I shows that the b-dimensional vector space of eigenfunctions of (3) decomposes into a three-dimensional subspace of odd parity and a $(b - 3)$-dimensional subspace of even parity with corresponding block-diagonal forms. No simple properties follow from this partial diagonalization.

Analogous reflection symmetries are present in models based on the square lattice such as the nine-bit thermal lattice gas [16]. One symmetry is a reflection $x \leftrightarrow -x$ for $\mathbf{k} = (0, k)$, or equivalently $y \leftrightarrow -y$ for $\mathbf{k} = (k, 0)$. The eigenspace of odd parity is again three dimensional, and the secular equation factorizes into a cubic equation and into one of degree 6. A second reflection symmetry $(x \leftrightarrow y)$ is present for $\mathbf{k} = (k, k)/\sqrt{2}$. The eigenspace of odd parity is again three dimensional, with similar consequences for the secular equation. None of these reflection symmetries lead to simple properties of the eigenvalue spectrum.

V. DISCUSSION

The eigenvalue spectra of the kinetic equation for single-particle-type fluctuations in a lattice gas as a function of the wave vector have been investigated both numerically and analytically. Most of the $\mathbf{k}$ interval is only accessible by numerical methods. Analytical results can be obtained by perturbative methods when the wavelength is large or small compared to the mean free path ℓ_0. Depending on the relevant $\mathbf{k}$ vector we distinguish a (generalized) hydrodynamic regime ($k\ell_0 \ll 1$), a kinetic regime ($k\ell_0 \simeq 1$), and a free-particle or Knudsen regime ($k\ell_0 \gg 1$).

Of paramount interest to fluid dynamics is the hydrodynamic regime, controlled by long-lived collective excitations with eigenvalues Re $z_\lambda(\mathbf{k}) \sim O(k^2)$, related to the conservation laws. A lattice gas is suitable for hydrodynamic simulations if some minimal criteria are satisfied: for wavelengths $\lambda > \lambda_h$, where λ_h should be on the order of a few lattice units, (i) the kinetic excitations should decay rapidly compared to the hydrodynamic ones and (ii) the transport coefficients appearing in the decay rates of the hydrodynamic modes should be independent of $\mathbf{k}$. According to these criteria the athermal FHP-III and the thermal 19-bit models are suitable for simulations, but the athermal FHP-I and the thermal nine-bit square lattice gas are not, because for lattices up to 250×250 their time dependence is totally dominated by nonlocal, i.e., $\mathbf{k}$-dependent, hydrodynamics.

For $\lambda < \lambda_h$ we are in the generalized hydrodynamics regime, where the speed of sound and transport coefficients (viscosities, heat diffusivity) become $\mathbf{k}$ dependent (see Figs. 3, 4, 6, and 7). This implies that the stress tensor and heat current are nonlocal functions of the gradients of flow field and temperature. These calculations are nonpertubative, and extend beyond the Chapman-Enskog expansion.

We have shown the necessity of using the concepts of generalized hydrodynamics for explaining some older simulation results obtained for six-bit FHP lattice gases with a small number of allowed collisions [7,8]. In particular we have resolved the puzzling observations of a negative bulk viscosity in Refs. [7,8]. We have also shown that the strong dispersion of the sound damping coefficient observed in Ref. [22] can be explained in a quantitative manner from the (numerically determined) eigenvalue spectrum of the Boltzmann equation.

The spectrum is an ideal tool to investigate the isotropy of the lattice gases. The isotropy of lattice gases defined on triangular lattices, is limited to small $|\mathbf{k}|$ values, as is illustrated in Figs. 2–4. For example, the data in Fig. 4 for $\nu(\mathbf{k})$ and $2\Gamma(\mathbf{k})$ (both theoretical and from simulations) would essentially have coincided if simulations had been performed at a $\mathbf{k}$ vector rotated over $\frac{1}{6}\pi$ with respect to a nearest-neighbor vector. On square lattices strong anisotropies occur, as illustrated in Fig. 6. The damping constant of the shear mode may differ by a factor of 2, depending on the direction of the $\mathbf{k}$ vector.

The spectra very clearly exhibit the existence of spurious conservation laws, which give rise to soft modes at finite wave numbers, as can be seen in the middle of the k interval in Figs. 2(a) and 2(c). Thermal lattice gases show an extra soft long-wavelength mode, the heat diffusion mode.

In lattice gases showing phase separation [9–12] the spectrum shows an instability of the Cahn-Hilliard type [13], caused by sound modes having Re $z_\pm > 0$ for wavelengths exceeding a certain value. The spectrum has been used to predict the wavelength and time scale of the onset of coarsening in phase separation [11,12].

The analysis presented in this paper is based on the linear Boltzmann equation, which accounts for short-ranged spatial correlations (i.e., $\mathbf{k}$-dependent transport coefficients), but neglects all memory effects. Therefore the present theory does not yield any frequency-dependent transport coefficients. However, if Eq. (1) would be extended to include ring collisions, then memory effects and long-time tails would be present, and the linearized collision operator Ω in Eq. (3) would become wave-number and frequency dependent. Still, the quantitative effects of long-time tails are very small [23,24].

In concluding this paper we emphasize that our discussion has been restricted to the more generic features of the eigenvalue spectra of single-particle fluctuations,

using an analysis based on mean-field theory. The main importance of analyzing the spectral properties is that they provide clear and crucial information about the basic criteria that lattice gases have to satisfy in order to qualify as models for nonequilibrium fluids, i.e., the existence of a sufficiently large range of wave numbers with strictly local transport coefficients, the isotropy of the fluid dynamic equations, the absence of spurious invariants, and the linear stability of spatial fluctuations.

ACKNOWLEDGMENTS

It is a pleasure to thank R. Brito for many stimulating discussions. One of us (H.J.B.) is financially supported by the Stichting voor Fundamenteel Onderzoek der Materie (FOM), which is sponsored by the Nederlandse Organistie voor Wetenschappelijk Onderzoek (NWO). S.P.D. also acknowledges FOM for financial support during a visit to the University of Utrecht.

[1] J. P. Boon and S. Yip, *Molecular Hydrodynamics* (Dover, New York, 1980).
[2] L. S. Luo, H. Chen, S. Chen, G. D. Doolen, and Y. C. Lee, Phys. Rev. A **45**, 7097 (1991).
[3] G. Zanetti, Phys. Rev. A **40**, 1539 (1989).
[4] M. H. Ernst, in *Liquids, Freezing and the Glass Transition*, edited by D. Levesque, J. P. Hansen, and J. Zinn-Justin (Elsevier Science, Amsterdam, 1991), p. 43.
[5] R. Brito and M. H. Ernst. J. Phys. A **24**, 3331 (1991).
[6] U. Frisch, D. d'Humières, B. Hasslacher, P. Lallemand, Y. Pomeau, and J.-P. Rivet, Complex Syst. **1**, 649 (1987) [reprinted in *Lattice Gas Methods for Partial Differential Equations*, edited by G. Doolen (Addison-Wesley, Singapore, 1990)].
[7] D. d'Humières and P. Lallemand, Complex Syst. **1**, 599 (1987).
[8] J. P. Rivet and U. Frisch, C.R. Acad. Sci. Paris **302**, 267 (1986).
[9] C. Appert and S. Zaleski, Phys. Rev. Lett. **64**, 1 (1990).
[10] M. Gerits, M. H. Ernst, and D. Frenkel, Phys. Rev. E (to be published).
[11] H. J. Bussemaker and M. H. Ernst, Proceedings of Statistical Physics, Berlin, 1992 [Physica A **194**, 258 (1993)].
[12] H. J. Bussemaker and M. H. Ernst, Proceedings of Euromech Colloquium No. 287 (Discrete Models in Fluid-Dynamics: Theory, Simulation, and Experiment) [Transport Theory Stat. Phys. (to be published)].
[13] K. Binder, in *Phase Transformations in Materials*, edited by P. Haasen, Materials Science and Technology Vol. 5 (VCH Verlag Weinheim, 1991).
[14] R. Brito, M. H. Ernst, and T. R. Kirkpatrick, in *Discrete Models of Fluid Dynamics*, Series on Advances in Mathematics for Applied Sciences, edited by A.S. Alves (World Scientific, Singapore, 1991), p. 198.
[15] P. Grosfils, J. P. Boon, R. Brito, and M. H. Ernst (unpublished).
[16] M. H. Ernst and S. P. Das, J. Stat. Phys. **66**, 465 (1992).
[17] I. M. de Schepper and E. G. D. Cohen, J. Stat. Phys. **27**, 223 (1982).
[18] D. d'Humières, P. Lallemand, and U. Frisch, Europhys. Lett. **2**, 291 (1986).
[19] S. P. Das and M. H. Ernst, Physica A **187**, 191 (1992).
[20] R. Brito, M. H. Ernst, and T. Kirkpatrick, J. Stat. Phys. **62**, 283 (1991).
[21] P. Resibois and M. de Leener, *Classical Kinetic Theory of Fluids* (Wiley, New York, 1977).
[22] P. Grosfils, J. P. Boon, and P. Lallemand, Phys. Rev. Lett. **68**, 1077 (1991).
[23] J. P. Boon, Physica D **47**, 3 (1991).
[24] M. A. van der Hoef and D. Frenkel, Physica D **47**, 191 (1991).